RESEARCH ARTICLE

ADVANCED OPTICAL MATERIALS
www.advopticalmat.de

Continuously Geometrical Tuning to Boost Circular Dichroism in 3D Chiral Metamaterials

Qiang Chen, Yawei Wu, Yongzhi She, Yilong Zhao, Jinlong Yang, Lijuan Chen, Peiwu Liu, Min Wu, Changgan Zeng, Zeming Qi, Chuansheng Hu, Hengjie Liu, Ying Xiong, Yangchao Tian, Yang Chen, Hongbing Cai,* Nan Pan,* and Xiaoping Wang*

Chiral metamaterials possess unique optical chiral responses, and the attainment of remarkable intrinsic chirality typically necessitates the disruption of their mirror symmetry to facilitate cross-coupling between electric and magnetic dipoles. However, achieving such symmetry breaking in a flexible and controllable manner remains challenging due to the limited range of applications afforded by available methodologies. Here, a method is proposed for fabricating robust three-dimensional (3D) chiral metamaterials by projecting arbitrary planar chiral metasurfaces onto on-demand height-tunable 3D silicon structures, thereby effectively modulating their optical chiral responses through continuously tuning the degree of cross-coupling between dipoles. Experimental and simulation results demonstrate this approach's ability to precisely control circular dichroism (CD) from a non-chiral state to various activated and enhanced chirality. Enhancing CD with high precision and continuous control manners can naturally provide an advanced opportunity and platform for the future design and actual applications of chiral optical systems.

1. Introduction

Chirality is a geometric property that refers to an object's inability to overlap with its mirror image through translation or rotation.[1] Chiral objects can exhibit remarkably different optical responses; for example, the divergence in the absorption of left-handed circularly polarized (LCP) and right-handed circularly polarized (RCP) light caused by the difference in the imaginary part of the refractive index is so-called circular dichroism (CD).[2–4] Constructing chiral metamaterials with on-demand CD value holds enormous significance in optical devices, sensors, life science, analytical chemistry, and medicine,[5–15] which can, in principle, be designed by tuning their cross-coupling of electrical and magnetic responses.[16–18] Benefiting from the continuous progress of nanofabrication technologies, the strategies and methods for preparing various novel metamaterials with higher optical chirality are developing rapidly. Generally, two mainstream design routes exist to obtain chiral response using the cross-coupling of electric and magnetic response. On the one hand, even planar chiral metasurface can get giant extrinsic chirality,[16,17,19] producing similar CD signals to intrinsic chiralit[20,21] under the oblique incidence of circularly polarized light (CPL). However, extrinsic chirality requires

Q. Chen, Y. Wu, C. Zeng, H. Cai, N. Pan, X. Wang
Hefei National Laboratory for Physical Sciences at the Microscale
University of Science and Technology of China
Hefei, Anhui 230026, China
E-mail: richard.cai@ntu.edu.sg; npan@ustc.edu.cn

Q. Chen
USTC Center for Micro- and Nanoscale Research and Fabrication
University of Science and Technology of China
Hefei, Anhui 230026, China

Y. Wu, Y. Chen
Chinese Academy of Sciences Key Laboratory of Mechanical Behavior and Design of Materials
Department of Precision Machinery and Precision Instrumentation
University of Science and Technology of China
Hefei, Anhui 230026, China
E-mail: cyang_phys@ustc.edu.cn

Y. She, Y. Zhao, J. Yang, P. Liu, M. Wu, C. Zeng, X. Wang
Department of Physics
University of Science and Technology of China
Hefei, Anhui 230026, China

L. Chen, Z. Qi, C. Hu, H. Liu, Y. Xiong, Y. Tian
National Synchrotron Radiation Laboratory
University of Science & Technology of China
Hefei, Anhui 230029, China

H. Cai
Division of Physics and Applied Physics
School of Physical and Mathematical Sciences
Nanyang Technological University
Singapore 637371, Singapore

The ORCID identification number(s) for the author(s) of this article can be found under https://doi.org/10.1002/adom.202400593

DOI: 10.1002/adom.202400593

activation by oblique incidence, which limits its application in integrated optics such as on-chip chiral emission and polarized photodetection.[5,22] On the other hand, numerous efforts have been made to achieve substantial intrinsic chirality by constructing 3D chiral metamaterials straightforwardly, including direct laser writing and subsequent electroplating,[5,23,24] stacking multilayer structures via electron beam lithography (EBL),[25–27] using a physical mask to grow materials,[28] controllably linking small nanoparticles together by self-assembly,[29–31] tilted angle etching,[22,32] in situ cutting and buckling a suspended metal film with programmed ion beam irradiation,[33–35] stencil lithography on a curved surface,[36,37] and so on. 3D chiral metamaterials can exhibit robust and remarkably enhanced intrinsic chirality, but the complexities of their fabrication processes pose challenges for high-precision and high-yield fabrication; the inadequate structural and mechanical stabilities also hinder the further on-chip integration with other materials, and the still limited controllability leads to the inability to achieve flexible and continuous control of the chiral response. Therefore, many constraints and drawbacks in preparing 3D chiral metamaterials with robust and controllable intrinsic chirality have impeded their further practical applications.

Here, we propose a method to manipulate the CD response by precisely projecting an arbitrary planar chiral metasurface onto spherical crown silicon bases with different heights and transforming them into robust 3D chiral metamaterial. First, most high-precision micro and nano processes, such as EBL and reaction ion etching, are two-dimensional (2D) methods. Our approach benefits from manufacturing on a non-planar/curved surface, realizing the preparation of 3D chiral metamaterials with high resolution using a 2D processing method. Second, silicon bases' height and aspect ratio can be continuously and precisely controlled, guaranteeing the excellent tuning of the CD response of the final structure from scratch to gradually increase without changing the graphic design. In addition, the support of robust silicon bases endows the upper 3D chiral metamaterials with good structural and mechanical stability, thus facilitating the on-chip multiple integrations with other materials. Moreover, not only arbitrary planar metasurfaces can be transformed into 3D chiral metamaterials on demand, but the deposited materials and compositions can also be arbitrarily selected on demand, like using phase change materials[38] to achieve tunable or switchable functionalities. Finally, the chiral structure manufactured by this scheme may satisfy the two mechanisms of chiral nanostructure and superchiral near field in the nanophotonic mechanisms.[10] This achievement showcases its potential for chiral sensors, which are expected to play an essential role in clinical, chemical, and biological research.

2. Results

To start with, it is essential to note that the physical origin of the optical chiral response in some metamaterials arises from the cross-coupling of electric and magnetic dipoles in parallel directions under dipole approximation.[35] According to Rosenfeld's calculation,[18,39] the condition of optical chiral response can be written as:

$$\mathbf{p} \cdot \mathbf{m} \neq 0 \tag{1}$$

where **p** and **m** are electric and magnetic dipole moments, respectively. One example of a planar chiral metasurface: the split-ring resonator (SRR), as shown in **Figure 1**a. When polarized light is incident normally, an electric dipole moment can be induced in the gap. The charge oscillations follow the bending of the structure, resulting in an induced ring current. Thus, the structure produces a magnetic dipole moment pointing out of the plane. By lifting one end of SRR, as depicted in Figure 1b, the orthogonality of the dipole moment generated by the structure is eliminated, resulting in $\mathbf{p} \cdot \mathbf{m} \neq 0$ and the structure having chirality. However, in other planar structures, such as fourfold rotational symmetry structure, it is known that only tangential current exists when the circularly polarized light is incident normally. Consequently, the resultant magnetic dipole moment always points out of the plane. It is orthogonal to the in-plane electric dipole moment, which makes them uncoupled and leads to a lack of chirality, as shown in Figure 1c. By inducing a bulge in the middle of the structure, we can alter the chirality from zero to some value by making the electric and magnetic dipoles generated by the structure non-orthogonal, as illustrated in Figure 1d.

We have designed the process depicted in Figure 1e to realize the cross-coupling of electric and magnetic dipoles discussed above. We obtain cylindrical patterns through EBL on intrinsic silicon with marks and coated with poly(methyl methacrylate) (PMMA) resist, as shown in Figure S1a (Supporting Information). To ensure the continuity of the upper pattern, we annealed the cylindrical PMMA, forming a spherical crown resist base with a gradual change in height, as illustrated in Figure S1b (Supporting Information). Figure S2 (Supporting Information) shows the influence of different annealing temperatures and spinning parameters on fabricating a spherical crown e-beam resist pattern. Then, we employed inductively coupled plasma (ICP) etching to transfer the spherical crown pattern to the intrinsic silicon substrate to create the spherical crown silicon base, as shown in Figure S1c (Supporting Information), which makes the base and substrate homogeneous and reduces the impact of different materials during the measurement process. The scanning electron microscope (SEM) images of the annealed PMMA and the etched silicon substrate demonstrate the uniformity of the silicon substrate replication of the PMMA pattern. Moreover, the height of the silicon base can be accurately controlled by the ICP process. The etching rate ratio between PMMA and silicon during ICP etching is calculated and presented in Figure S3 (Supporting Information). Table S1 (Supporting Information) shows different etching rate ratios obtained by different etching parameter settings. To ensure the uniformity of the thickness of the film on an uneven substrate, we transferred the PMMA film peeling off with potassium hydroxide solution to the etched silicon substrate. Through precise EBL alignment and electron beam evaporation (EBE), we have successfully projected a variety of planar chiral metasurface capable of generating strong local surface plasmon resonance onto spherical crown silicon base and transformed it into 3D chiral metamaterial with strong intrinsic chirality. A detailed description of the process steps can be found in the Experimental Section. Using the above methods, we have successfully fabricated several different 3D chiral metamaterials arrays, including single 3D metallic spirals, double-spiral, and fourfold rotational symmetry metallic metamaterials. The SEM images of these arrays are shown in Figure 1f–h, respectively.

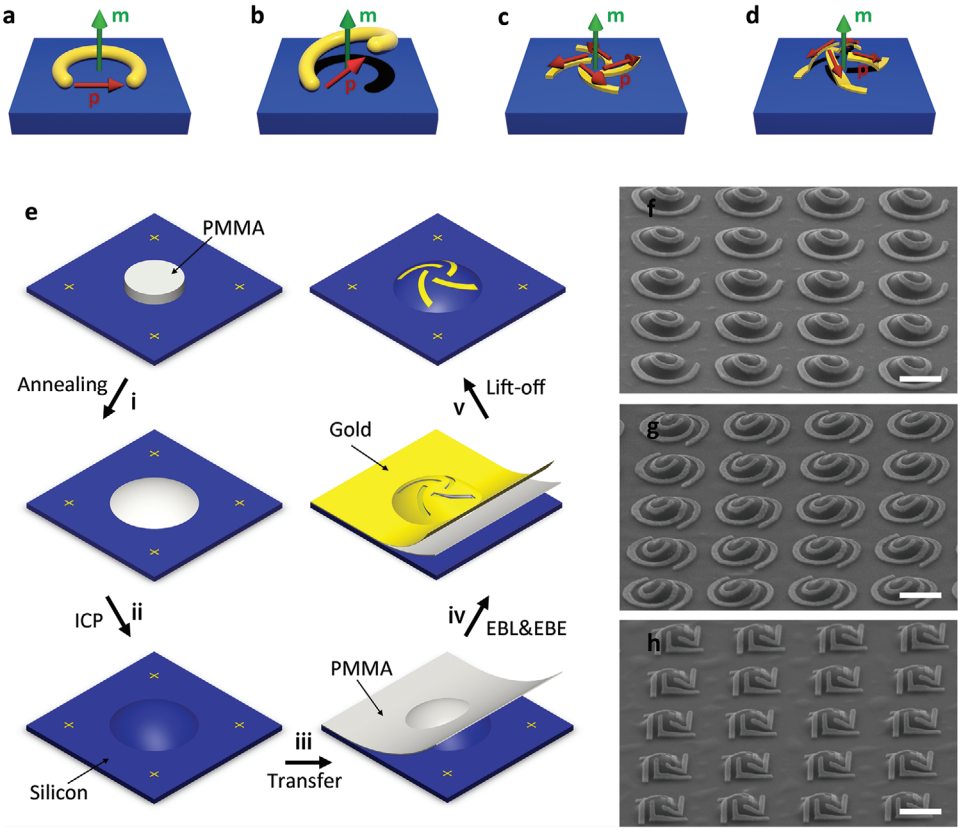

Figure 1. Fabricating 3D chiral metamaterials. a,c) 2D planar chiral metasurfaces. b,d) 3D chiral metamaterials. The images show the direction of the electric dipole moment (**p**, red arrow) and magnetic dipole moment (**m**, green arrow) generated by the structure under the normal incidence of circularly polarized light. These moments are illustrated as simple arrows for ease of understanding. e) The schematic illustration of fabricating 3D chiral metamaterials. **i**) The electron-beam resist PMMA is annealed to transform from a cylindrical to a spherical crown shape after EBL exposure. **ii**) The PMMA patterns are transferred to the silicon substrate by ICP etching. **iii**) The PMMA membrane stripped from the Si/SiO_2 wafer is transferred onto the etched silicon substrate. **iv**) The transferred PMMA membrane is exposed by EBL with alignment, and electron beam evaporation is performed. **v**) A standard lift-off procedure is performed. Tilt-view SEM images of single 3D metallic spirals f), double-spiral g), and fourfold rotational symmetry h) metallic metamaterials. The scale bars in the images are 1 µm.

To investigate the CD of the chiral structure, we selected the fourfold rotational symmetry metamaterials for a detailed study, which can avoid anisotropy effects that lead to polarization conversion.[27,40] We selected appropriate parameters to evaluate the extent to which the upper and lower structure centers deviate due to instrument error. Figure S4 (Supporting Information) shows that the CD of the slightly mismatched structure exhibited minimal effect, exhibiting only a marginal disparity in intensity. This observation underscores the scheme's remarkable tolerance for alignment accuracy and its potential for large-scale manufacturing of 3D chiral metamaterials with high reproducibility. 2D right-handed (RH), 3D left-handed (LH), and RH metamaterials arrays with lattice periodicity of 2 µm are fabricated, as shown in **Figure** 2a,b, where the central part of the 3D structure is fitted to the spherical crown silicon base. Due to the precise directionality of the exposure and metal deposition process, the projection size of 2D and 3D structures on the silicon substrate plane remained consistent. As the structural parameters of a unit cell shown in Figure 2c, the short side of the "L" type measured ≈500 nm, the long side ≈800 nm, and the width roughly 120 nm on the projection plane. Before the 30 nm gold film was deposited, a 5 nm titanium film was deposited as an adhesive layer. Optical measurements indicate that the 2D RH structure exhibited no CD effect under normal incidence, as plotted in Figure 2c. In comparison, the experimental 3D structure in Figure 2a,b exhibits apparent CD effects, in which the CD spectra of LH and RH 3D structures show nearly opposite signs with similar amplitudes; a CD peak can be seen at a wavelength of 2.35 µm, as the curves plotted in Figure 2c. Here, we define $CD = (T_R - T_L)/(T_R + T_L)$, where T_R and T_L denote the transmission of the structure under RCP and LCP light incidence, respectively. The calculation procedure of the experimental data and the transmission spectrum corresponding to the CD curve of 2D and 3D chiral structures are shown in Figures S5 and S6 (Supporting Information). As plotted in Figure 2d, the simulation results show the line shape of the simulated CD curve; the peak position and intensity agree well with the experimental results. The simulated CD curve fluctuates at a wavelength of 2 µm, which may be due to Wood's anomalies[35,41] and can be more clearly observed in the transmission curve, as shown in Figure S6d–f (Supporting Information). Periodic structures can show abrupt changes in reflection, which will be eliminated by the inhomogeneity of the period caused

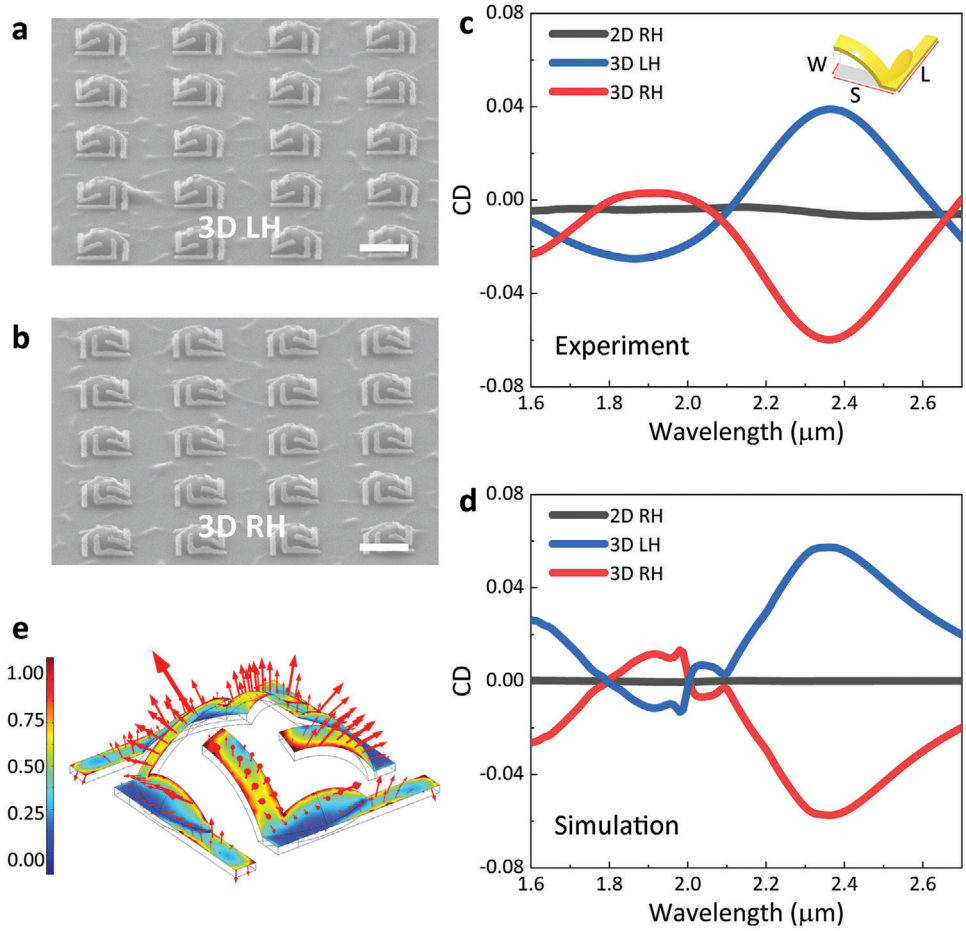

Figure 2. Characterization of CD in chiral metamaterials. a,b) Tilt-view SEM images of 3D LH and RH chiral metamaterials with a periodicity of 2 μm. The scale bar is 1 μm. c,d) Measured and simulated CD in transmission versus wavelength for 2D RH, 3D LH, and 3D RH chiral metamaterials, respectively. CD is defined as CD $= (T_R - T_L)/(T_R + T_L)$. Inset is the structural parameters of a unit cell. The length of the short side of the "L" shaped structure "s" is ≈500 nm, the long side "l" is ≈800 nm, and the width of the "L" shaped structure "w" is ≈120 nm. e) Normalized electric field amplitude distribution of a 3D chiral metamaterial with a height of 300 nm simulated under RCP incidence with a wavelength of 2.35 μm. The arrows indicate the direction of the electric field.

by micro-nano processing errors in the experiment. Both experimental and simulation results unambiguously demonstrate that the introduction of 3D structures through the above methods remarkably enhances optical chirality compared with the 2D counterpart, data over a broader range shown in Figure S7 (Supporting Information).

Aiming to comprehend the coupling of electric and magnetic dipoles in generating CD responses in our structure, we conducted simulations to analyze the distribution of the normalized electric field amplitude on the 2D and 3D chiral metamaterials under the normal incidence of different CPL at their characteristic wavelengths, as shown in Figure S8 (Supporting Information). Upon comparison, it is evident that the normalized electric field amplitude under RCP light incidence is remarkably higher than that under LCP light incidence, which matches the phenomenon of lower transmittance under RCP light incidence in Figure S6c,d (Supporting Information), indicating the differential absorption of the structure for different CPL, and the CD response of the structure. Then, we just focus on the distribution of the normalized electric field amplitude on the 3D chiral metamaterial under RCP light incidence, as shown in Figure 2e. Compared with the 2D structure, the difference in the normalized electric field amplitude of the 3D structure is mainly in the convex part, while the part in the plane remains consistent. Thus, our subsequent analysis concentrates on the convex part of the main structure, specifically the short arm part of the "L" shaped structure. The complexity of our 3D structure prevents it from being adequately explained and analyzed by the coupled oscillator model.[27] From the short arm's normalized electric field amplitude distribution, we can approximate it as an electric dipole with a direction downward along the structure. Due to the fourfold symmetry of the structure, the stacking of four electric dipole moments (**p**) induces an upward-oriented magnetic dipole moment (**m**), as shown in Figure 1c,d. The simulation results for the normalized magnetic field amplitude distribution of the Bz component (Figure S9, Supporting Information) confirm our suspicions. In a 2D structure, **p** and **m** are perpendicular, and no chirality is generated, but in a 3D structure, **p** and **m** form obtuse angles and are coupled with each other to produce chiral responses. Moreover, as the height of the base increases, the angle between

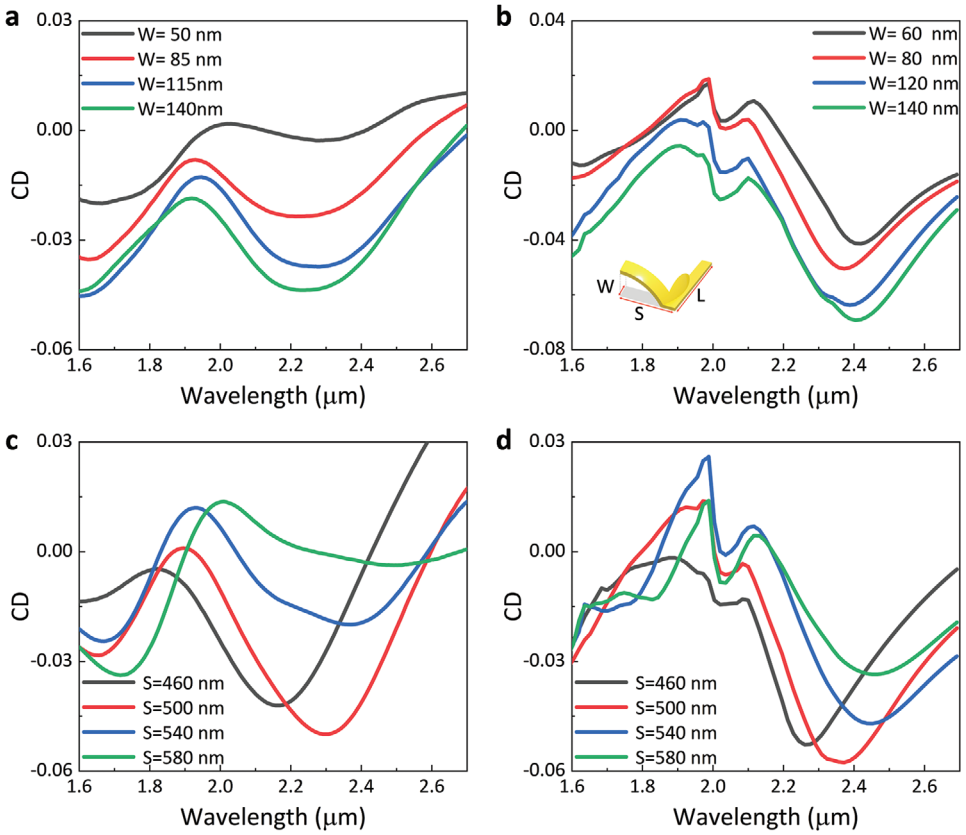

Figure 3. CD curves of samples at different upper structure parameters. a,b) Experimentally measured and simulated CD curves for chiral metamaterials of different widths, respectively. The structural parameters of a unit cell are illustrated in the inset. The CD peak intensity increases with the growth of the width of the structure. c,d) Experimentally measured and simulated CD curves for chiral metamaterials of different short side lengths, respectively. The CD peak position redshifts with the short side lengths of the structure growing, and the experimental spectra are in good agreement with the simulated spectra.

the **p** and **m** becomes larger until it tends to be parallel, which could result in more robust chiral responses.

We have investigated the functional range and tunability of chiral metamaterials produced by the above preparation schemes. First, we delved into the impact of upper structure parameters on the chiral metamaterial's CD. According to the approximate model mentioned above, the chirality of the structure primarily comes from the coupling of the electric dipole in a downward direction along the short side structure and the magnetic dipole pointing out of the plane. As the structure's width increases, the surface current's total strength increases, leading to stronger electric and magnetic fields and increased CD intensity, as shown in **Figure** 3a,b. However, the short side length remains unchanged with an increase in width, resulting in no significant change in CD's characteristic wavelengths or peak position. On the other hand, an increase in short side length leads to a redshift in the peak position of CD, as illustrated in Figure 3c,d. It's important to note that both the morphology and total surface current intensity of the 3D structure change with an increase in short edge length, leading to a non-monotonic change in CD intensity, with the maximum peak intensity observed at a short side length of 500 nm. The corresponding structures' SEM images are presented in Figures S10 and S11 (Supporting Information). Then, we scaled the size and period of the structure to different proportions, using the structure depicted in Figure 2b as a reference. Due to the limited range of wavelengths in the experiment, we only tested samples with scaling ratios of 0.75, 1, and 1.25. The SEM images of the corresponding structures are shown in the illustrations in **Figure** 4a. From the experimental (Figure 4a) and simulated (Figure 4b) data, it is evident that with the increase of scaling ratio, the feature size increases and the CD peak redshifts. In summary, scaling can obtain the desired CD peak according to the corresponding CD peak demand. We can also enhance the CD peak intensity by increasing the width of the upper structure.

In addition, we can manipulate the angle between **p** and **m** by adjusting the height of the spherical crown silicon base to control the CD response of the structure, which highlights the flexibility of our proposed fabrication scheme for 3D chiral metamaterials. As mentioned above, varying etching parameters can achieve different PMMA to silicon etching rate ratios. Consequently, we can use other etching parameters to etch the same substrate or use the same etching parameters to etch different substrates to obtain silicon bases of different heights. Figure S12 (Supporting Information) shows the circular truncated cone-shaped silicon substrate formed after etching for 30 s and the spherical crown silicon substrate formed after exactly etching off the upper PMMA layer at different etching rates and ratios. Then, various 3D RH

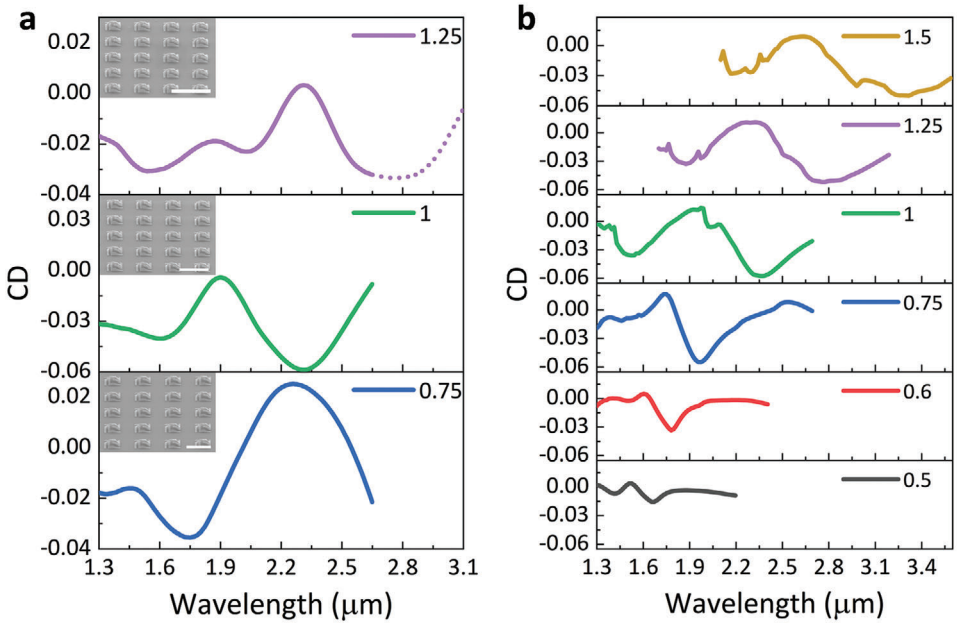

Figure 4. CD curves of structures with different sizes under equal scaling. a) Experimentally measured CD curves for chiral metamaterials of different sizes, respectively. The dashed line serves as a visual representation indicating that the measured data surpasses the designated measurement range and is solely intended for reference purposes. Insets are tilt-view SEM images of the structures. The scale bars in the images are 2 μm. b) Simulated CD curves for chiral metamaterials of different sizes, respectively. The CD peak position redshifts with the growing scaling ratio and the trend of the experimental spectra is consistent with that of the simulated spectra.

chiral structures were constructed by projecting planar RH structures onto spherical crown silicon substrates of different heights. **Figure** 5a,b shows the SEM images of 3D RH chiral metamaterial at 190 and 280 nm, and Figure 5c shows the height curves of different 3D RH chiral metamaterial. More SEM images of varying height samples can be found in Figure S13 (Supporting Information). To explore the trend of chirality changing with height, we measured the CD response of chiral metamaterials with different heights, as shown in Figure 5d. The structure's height is from 0 to 98, 190, 280 nm, and the peak intensity of CD gradually increases from 0% to 1.6%, 3.5%, and 6%, respectively. The redshift of the CD peak with increasing base height can be attributed to the elongation of the actual length of the short arms due to the height increase. Additional CD curves corresponding to samples of different heights can be found in Figure S14 (Supporting Information). The simulated results of CD response for chiral metamaterials with 0, 100, 200, and 300 nm heights are presented in Figure 5e. The peak intensity of the CD curve and the trend of peak position changing with height are almost consistent with the experimental results. The minor difference between experimental and simulation results may stem from the error introduced during the experimental process. The above intensity trend of the CD curve indicates that we can effectively control the CD response of chiral metamaterials by increasing the height of the silicon base.

3. Conclusion

We have developed a well-controlled scheme for the fabrication of robust 3D chiral metamaterials based on the principle that the cross-coupling of electric and magnetic dipoles induces intrinsic optical chiral responses, through which we can transform an arbitrary planar chiral metasurface into a robust 3D chiral structure by precisely projecting the former onto a patterned 3D silicon base of different heights on demand. Specifically, we have systematically investigated the geometrical tuning of optical chirality by fabricating fourfold rotational symmetry 3D chiral structures. The experimental and simulation results verify the correctness of our proposed electric and magnetic dipole coupling model, and we can use the structural parameters of chiral metamaterials to control the surface current intensity and manipulate the degree of coupling between the electric and magnetic dipoles. As a result, the strength and wavelength of the optical chiral response can eventually be well-tuned. The proposed approach has the potential to pave the way for the development of metamaterials with higher chirality and actively modulated optical chiral responses. This, in turn, presents opportunities for realizing chirality modulation or switching, sensing, and expanding the applications for optical devices.

4. Experimental Section

Sample Fabrication: The PMMA film was produced beginning with the spinning coating of PMMA (950K, 4 wt% in chlorobenzene) on a Si substrate at an initial rotary speed of 600 rpm for 10 s and then at 2000 rpm for 30 s. Then, the sample was baked on a hot plate at 180 °C for 2 min, and the final thickness of the PMMA membrane was ≈350 nm. All exposure procedures were prepared using a standard EBL process. For development, the exposed sample was inserted into a solution of isopropyl alcohol (IPA) and methyl isobutyl ketone (MIBK) of a 3:1 volume ratio for 60 s and then inserted into IPA for 40 s before blow-drying it with a flow of nitrogen. The PMMA patterns were annealed in an oven at 120 °C for 1 hour and cooled to room temperature naturally.[37] Due to the glass transition

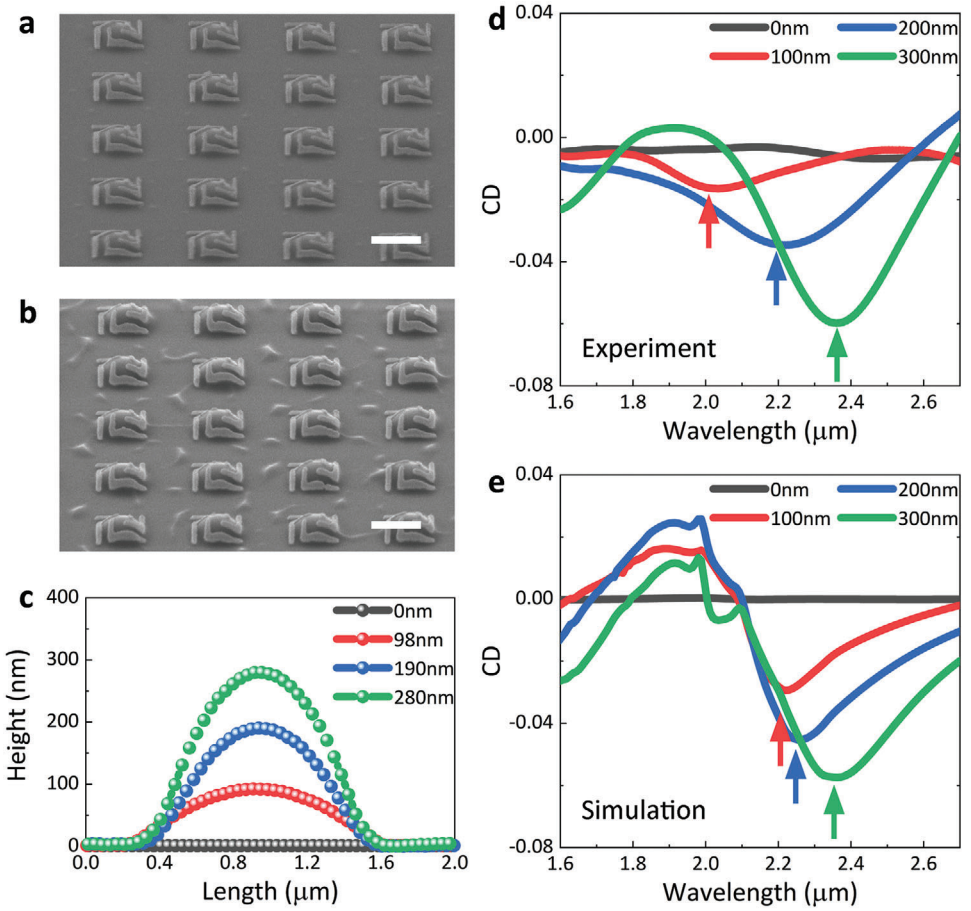

Figure 5. Modulating the structural chirality with the height of the silicon base. a,b) Tilt-view SEM images of 3D chiral metamaterials with varying silicon substrate heights of 190 and 280 nm. Scale bar, 1 μm. c) Height curves of individual structures of different silicon substrates. d,e) Experimentally measured and simulated CD curves for chiral metamaterials of different heights, respectively. The CD peak intensity increases and peak position redshifts with the height of the base growing, and the experimental spectra are in good agreement with the simulated spectra.

of the PMMA, the PMMA's cylindrical structure changed to a spherical crown shape. The ICP etching system implemented the etching procedure (Oxford, Plasma System 100 ICP 380). Height measurements were all obtained by atomic force microscopy (AFM). Potassium hydroxide solution was used at 95 °C to peel PMMA films spin-coated on Si/ SiO_2 substrate in a petri dish for subsequent transfer operations. To ensure the accurate alignment of the upper pattern with the lower structure, the mark to calibrate the exposure position was used during each EBL exposure. After EBL exposure, the metallic 3D metamaterials of 35 nm thickness (5 nm titanium and 30 nm gold film) were deposited by the E-beam evaporator system with a rate of 0.6 Å s^{-1}. A standard lift-off procedure in acetone was performed.

Infrared Transmission Spectra Characterization: Micro-area transmission spectra were collected at room temperature on a Fourier transform infrared (FTIR) spectrometer (Bruker IFS 66v, Germany) on the infrared beamline station (U4) at the National Synchrotron Radiation Laboratory (NSRL), Hefei, China. All the IR spectra were measured in transmission mode at the step resolution of 2 cm^{-1}. The specific area for Figures 2c and 3a–c, Figures 4a and 5d, Figures S4–S7 and S14 (Supporting Information) were ≈10 μm^2 × 10 μm^2. For the measurement of CD, a linear polarizer (1000 to 3000 nm; Thorlabs) and a superachromatic quarter-wave plate (600 to 2700 nm; Thorlabs) were inserted into the input optical path at specific orientations.

Numerical Simulations: All the simulations in this work were conducted by a finite-element-method solver in COMSOL Multiphysics. Periodic boundary conditions were applied in the x and y directions, whereas perfectly matched layers were used in the z-direction. The refractive index of gold was taken from the Brendel–Bormann model,[42] while that of Si was set as 3.33. The geometric parameters used in the simulation were the same as the values from the SEM images for each sample.

Supporting Information

Supporting Information is available from the Wiley Online Library or from the author.

Acknowledgements

The authors acknowledge the financial support from the Strategic Priority Research Program of CAS (Grant No. XDC07010000), the MOST of China (Grant No. 2016YFA0200602), the National Natural Science Foundation of China, and the Anhui Initiative in Quantum Information Technologies (Grant No. AHY090200). This work was partially carried out at the USTC Center for Micro and Nanoscale Research and Fabrication; the authors thank the Hefei Synchrotron Radiation Facility (BL01B Infrared spectroscopy and microspectroscopy).

Conflict of Interest

The authors declare no conflict of interest.

Data Availability Statement

The data that support the findings of this study are available from the corresponding author upon reasonable request.

Keywords

3D chiral metamaterials, 3D fabrication, circular dichroism, intrinsic chirality

Received: March 1, 2024
Revised: April 22, 2024
Published online: May 16, 2024

[1] L. D. Barron, *Molecular light scattering and optical activity*, Cambridge University Press, Cambridge, **2004**.
[2] M. Hentschel, M. Schaeferling, X. Duan, H. Giessen, N. Liu, *Sci. Adv.* **2017**, *3*, e1602735.
[3] M. Qiu, L. Zhang, Z. Tang, W. Jin, C. W. Qiu, D. Y. Lei, *Adv. Funct. Mater.* **2018**, *28*, 1803147.
[4] Y. Luo, C. Chi, M. Jiang, R. Li, S. Zu, Y. Li, Z. Fang, *Adv. Opt. Mater.* **2017**, *5*, 1700040.
[5] J. K. Gansel, M. Thiel, M. S. Rill, M. Decker, K. Bade, V. Saile, G. von Freymann, S. Linden, M. Wegener, *Science* **2009**, *325*, 1513.
[6] C. Menzel, C. Helgert, C. Rockstuhl, E. B. Kley, A. Tunnermann, T. Pertsch, F. Lederer, *Phys. Rev. Lett.* **2010**, *104*, 253902.
[7] M. Cen, J. Wang, J. Liu, H. He, K. Li, W. Cai, T. Cao, Y. J. Liu, *Adv. Mater.* **2022**, *34*, 2203956.
[8] L. Mao, K. Liu, S. Zhang, T. Cao, *ACS Photonics* **2020**, *7*, 375.
[9] E. Zor, H. Bingol, M. Ersoz, *Trac, Trends Anal. Chem.* **2019**, *121*, 115662.
[10] L. A. Warning, A. R. Miandashti, L. A. Mccarthy, Q. Zhang, C. F. Landes, S. Link, *ACS Nano* **2021**, *15*, 15538.
[11] E. Hendry, T. Carpy, J. Johnston, M. Popland, R. V. Mikhaylovskiy, A. J. Lapthorn, S. M. Kelly, L. D. Barron, N. Gadegaard, M. Kadodwala, *Nat. Nanotechnol.* **2010**, *5*, 783.
[12] J. P. Hall, P. M. Keane, H. Beer, K. Buchner, G. Winter, T. L. Sorensen, D. J. Cardin, J. A. Brazier, C. J. Cardin, *Nucleic Acids Res.* **2016**, *44*, 9472.
[13] W. Ma, H. Kuang, L. Xu, L. Ding, C. Xu, L. Wang, N. A. Kotov, *Nat. Commun.* **2013**, *4*, 2689.
[14] G. Wang, C. Hao, W. Ma, A. Qu, C. Chen, J. Xu, C. Xu, H. Kuang, L. Xu, *Adv. Mater.* **2021**, *33*, 2102337.
[15] Y. Chen, W. Du, Q. Zhang, O. Avalos-Ovando, J. Wu, Q. Xu, N. Liu, H. Okamoto, A. O. Govorov, Q. Xiong, C. Qiu, *Nat. Rev. Phys.* **2022**, *4*, 138.
[16] E. Plum, V. A. Fedotov, N. I. Zheludev, *Appl. Phys. Lett.* **2008**, *93*, 191911.
[17] E. Plum, X. Liu, V. A. Fedotov, Y. Chen, D. P. Tsai, N. I. Zheludev, *Phys. Rev. Lett.* **2009**, *102*, 113902.
[18] M. Schäferling, *Chiral Nanophotonics*, Springer, Switzerland **2017**.
[19] W. Liu, B. Wang, Y. Zhang, J. Wang, M. Zhao, F. Guan, X. Liu, L. Shi, J. Zi, *Phys. Rev. Lett.* **2019**, *123*, 116104.
[20] Z. Wang, L. Jing, K. Yao, Y. Yang, B. Zheng, C. M. Soukoulis, H. Chen, Y. Liu, *Adv. Mater.* **2017**, *29*, 1700412.
[21] M. V. Mukhina, V. G. Maslov, A. V. Baranov, A. V. Fedorov, A. O. Orlova, F. Purcell-Milton, J. Govan, Y. K. Gun Ko, *Nano Lett.* **2015**, *15*, 2844.
[22] Y. Chen, H. Deng, X. Sha, W. Chen, R. Wang, Y. H. Chen, D. Wu, J. Chu, Y. S. Kivshar, S. Xiao, C. W. Qiu, *Nature* **2023**, *613*, 474.
[23] A. Radke, T. Gissibl, T. Klotzbücher, P. V. Braun, H. Giessen, *Adv. Mater.* **2011**, *23*, 3018.
[24] J. K. Gansel, M. Latzel, A. Frölich, J. Kaschke, M. Thiel, M. Wegener, *Appl. Phys. Lett.* **2012**, *100*, 101109.
[25] N. Liu, H. Guo, L. Fu, S. Kaiser, H. Schweizer, H. Giessen, *Nat. Mater.* **2008**, *7*, 31.
[26] Z. Wang, H. Jia, K. Yao, W. Cai, H. Chen, Y. Liu, *ACS Photonics* **2016**, *3*, 2096.
[27] X. Yin, M. Schäferling, B. Metzger, H. Giessen, *Nano Lett.* **2013**, *13*, 6238.
[28] J. H. Han, D. Kim, J. Kim, G. Kim, P. Fischer, H. H. Jeong, *Adv. Mater.* **2023**, *35*, 2370239.
[29] A. J. Mastroianni, S. A. Claridge, A. P. Alivisatos, *J. Am. Chem. Soc.* **2009**, *131*, 8455.
[30] A. Kuzyk, R. Schreiber, Z. Fan, G. Pardatscher, E. M. Roller, A. Hogele, F. C. Simmel, A. O. Govorov, T. Liedl, *Nature* **2012**, *483*, 311.
[31] L. Zhang, T. Wang, Z. Shen, M. Liu, *Adv. Mater.* **2016**, *28*, 1044.
[32] Y. Chen, J. Gao, X. Yang, *Nano Lett.* **2018**, *18*, 520.
[33] S. Yang, Z. Liu, S. Hu, A. Jin, H. Yang, S. Zhang, J. Li, C. Gu, *Nano Lett.* **2019**, *19*, 3432.
[34] S. Yang, Z. Liu, H. Yang, A. Jin, S. Zhang, J. Li, C. Gu, *Adv. Opt. Mater.* **2020**, *8*, 1901448.
[35] Z. Liu, Du H., J. Li, L. Lu, Z. Y. Li, N. X. Fang, *Sci. Adv.* **2018**, *4*, eaat4436.
[36] H. Cai, Q. Meng, H. Ding, K. Zhang, Y. Lin, W. Ren, X. Yu, Y. Wu, G. Zhang, M. Li, N. Pan, Z. Qi, Y. Tian, Y. Luo, X. Wang, *ACS Nano* **2018**, *12*, 9626.
[37] H. Cai, Q. Meng, Q. Chen, H. Ding, Y. Dai, S. Li, D. Chen, Q. Tan, N. Pan, C. Zeng, Z. Qi, G. Liu, Y. Tian, W. Gao, X. Wang, *Adv. Mater.* **2020**, *32*, 2002570.
[38] T. Cao, L. Mao, H. Fan, M. Lian, J. Jia, Y. Su, H. Ren, *Adv. Opt. Mater.* **2023**, *11*, 2202239.
[39] A. Y. Zhu, W. T. Chen, A. Zaidi, Y. W. Huang, M. Khorasaninejad, V. Sanjeev, C. W. Qiu, F. Capasso, *Light-Sci. Appl.* **2018**, *7*, 17158.
[40] M. Kuwata-Gonokami, N. Saito, Y. Ino, M. Kauranen, K. Jefimovs, T. Vallius, J. Turunen, Y. Svirko, *Phys. Rev. Lett.* **2005**, *95*, 227401.
[41] G. Vecchi, V. Giannini, R. J. Gomez, *Phys. Rev. Lett.* **2009**, *102*, 146807.
[42] A. D. Rakic, A. B. Djurisic, J. M. Elazar, M. L. Majewski, *Appl. Optics* **1998**, *37*, 5271.